

#### **PAPER • OPEN ACCESS**

# A computational approach for the simulation of shape memory polymer-based structures via finite elements and mesh morphing

To cite this article: Corrado Groth et al 2025 Smart Mater. Struct. 34 075049

View the article online for updates and enhancements.

# You may also like

- Recent advances in vibration energy harvesting reinforced by bioinspired designs/structures
- Mohamed A A Abdelkareem, Xingjian Jing, Mohamed Kamal Ahmed Ali et al.
- <u>Shape memory polymers for neural interfaces: a mini-review</u>
  Lu Dai, Chenghao Zheng, Jizhou Song et
- Optimization of PLA/CF 4D printing parameters by Box–Behnken response surface method

Xianchao Zhang, Shaogang Liu, Pengfei Wang et al.



Smart Mater. Struct. 34 (2025) 075049 (12pp)

https://doi.org/10.1088/1361-665X/adf309

# A computational approach for the simulation of shape memory polymer-based structures via finite elements and mesh morphing

Corrado Groth<sup>1</sup>, Andrea Chiappa<sup>1</sup>, Marco Evangelos Biancolini<sup>1</sup> and Giulia Scalet<sup>2,\*</sup>

E-mail: giulia.scalet@unipv.it

Received 30 May 2025, revised 17 July 2025 Accepted for publication 22 July 2025 Published 31 July 2025



#### **Abstract**

Shape-memory polymers (SMPs) are a widely-used class of smart materials capable of recovering a pre-defined permanent shape from a deformed temporary configuration when exposed to external stimuli. A crucial step in this behavior is shape-programming, which enables the fixation of the temporary shape. Simulating this step through numerical models can be both computationally expensive and prone to inaccuracies. This is primarily due to the difficulty in identifying the appropriate set of boundary conditions needed to deform the structure into the desired temporary shape, often requiring multiple trial-and-error iterations. This paper proposes a computational approach that overcomes such a difficulty and enables an accurate simulation of the shape-memory cycle. The core innovation lies in the use of mesh morphing techniques to directly impose the temporary shape, thereby eliminating the need to determine complex mechanical loading conditions during the programming step. This method is integrated within a finite element framework and applied to a representative 4D printed structure. Numerical results confirm the robustness and accuracy of the approach, which replicates the recovery behavior of the SMP while significantly reducing computational effort in finding and applying the right set of boundary conditions. This work provides a valuable tool for the design of SMP systems.

Keywords: shape memory polymers, finite element method, mesh morphing, radial basis functions

Original Content from this work may be used under the terms of the Creative Commons Attribution 4.0 licence. Any further distribution of this work must maintain attribution to the author(s) and the title of the work, journal citation and DOI.

<sup>&</sup>lt;sup>1</sup> Department of Enterprise Engineering, University of Rome Tor Vergata, via del Politecnico 1, Roma 00133, Italy

<sup>&</sup>lt;sup>2</sup> Department of Civil Engineering and Architecture, University of Pavia, via Ferrata 3, Pavia 27100, Italy

<sup>\*</sup> Author to whom any correspondence should be addressed.

#### 1. Introduction

Shape-memory polymers (SMPs) are smart materials employed in a wide range of applications and components, including biomedical devices, drug delivery systems, engineered scaffolds for tissue engineering and regenerative medicine purposes, soft actuators, and self-deployable structures [1].

Their appeal lies in their remarkable ability to recover the original (permanent) shape from a deformed (temporary) one when exposed to an external stimulus such as heat, pH, or an electric field -a capability known as the shape-memory effect (SME). Among the different stimuli, the thermally-activated SME is the most extensively studied. In such a case, recovery occurs through direct or indirect heating above the so-called transition temperature,  $T_{\rm trans}$ , such as the glass transition or melting temperature.

The overall SME process -referred to as the shapememory cycle- typically involves two main stages: shapeprogramming and shape-recovery. As the names suggest, shape-programming is needed to fix the temporary shape, while shape-recovery to retrieve the permanent configuration from the temporary one. Moreover, depending on the polymer type and on the programming step applied to the material, SMPs can exhibit various forms of thermally-driven SME [2]. Specifically, the one-way SME allows recovery of the permanent shape from a single temporary shape upon heating (figure 1(A)). Here, shape-programming entails deforming the material above  $T_{\text{trans}}$  to achieve the temporary shape, then cooling it below  $T_{\text{trans}}$  under load to fix the temporary shape. The load is finally removed, and shape recovery is triggered by reheating the polymer above  $T_{\text{trans}}$  under load-free conditions. The multiple SME enables recovery from two or more temporary shapes (figure 1(B)). In both the one-way and multiple SME, the reset of the temporary shape(s) requires to reapply the programming step after recovery. Conversely, the two-way SME provides reversible switching between two temporary shapes solely through cyclic heating and cooling (figure 1(C)), without mechanical resetting.

Temporary shapes are not arbitrary, but known in advance; they are application-driven targets, and the programming step is essential to fix them. Thanks to the current advancements in additive manufacturing technologies, especially in 4D printing [3], personalized permanent shapes can be produced and then deformed into even more complex temporary shapes.

Constitutive modeling plays a crucial role in supporting the design and simulation of the entire shape-memory cycle in SMP-based structures. Numerous models have been proposed to capture the different SMEs, many of which are implemented within finite element frameworks. For a comprehensive overview, the reader is referred to review articles such as [4].

However, simulating the shape-memory cycle -especially the programming step- can be computationally demanding or imprecise for complex geometries. This is because a system of partial differential equations (PDEs) with carefully selected boundary conditions (e.g. mechanical loads or displacements along the domain boundary) has to be solved to obtain the target temporary shape from the permanent one. Identifying the correct set of boundary conditions leading to the target temporary shape often requires a difficult and inaccurate trialand-error approach, even in a numerical environment.

This paper addresses this challenge by proposing a computational approach that enables an accurate and robust finite element simulation of the shape-memory cycle in SMP-based structures.

The core idea presented in this work is to employ mesh morphing techniques to directly impose the desired temporary shape through the mechanical deformation, bypassing the need for complex and unknown boundary condition setups during the programming phase. To obtain an accurate control of the mesh deformation RBF Morph, a commercial Radial Basis Functions (RBF) based mesh morphing tool, is proposed in this work. RBF proved to be a powerful mesh deformation paradigm in several fields, ranging from shape optimization [5] to complex multiscale stress retrieval problems [6]. The displacement boundary conditions inferred by mesh morphing are then used to deform the material above  $T_{\text{trans}}$  with a precise temporary shape, then driving the finite element simulation of the full shape-memory cycle. The presented approach is here applied to a 4D printed structure made of a SMP featuring the one-way SME.

The paper is organized as follows. At first a theoretical background on RBF is given in section 2, then the proposed workflow is presented in section 3 describing the novel approach to deform the structure onto the temporary shape and the strategy to perform the numerical simulation of the shape-memory cycle. The presented method is finally demonstrated on a test case and results are discussed in section 4. Conclusions and perspectives are given in section 5.

#### 2. Theoretical background

This section is dedicated to first introduce the reader to the theory behind mesh morphing.

#### 2.1. RBFs

RBFs are mathematical tools designed to interpolate scalar values known only at discrete locations—referred to as source points—based on their mutual distances. The quality and behavior of the interpolation are influenced by both the selected RBF and the type of basis function employed. Specifically, RBFs are categorized according to the nature of their support—either global or compact—i.e. the region within which the function assumes non-zero values [7]. A selection of commonly used RBFs is presented in table 1.

RBFs are defined in an *n*-dimensional space and operate as functions of the distance between points, typically expressed using the Euclidean norm, particularly in morphing applications.

To determine the interpolation coefficients, a linear system of equations—whose size equals the number of source

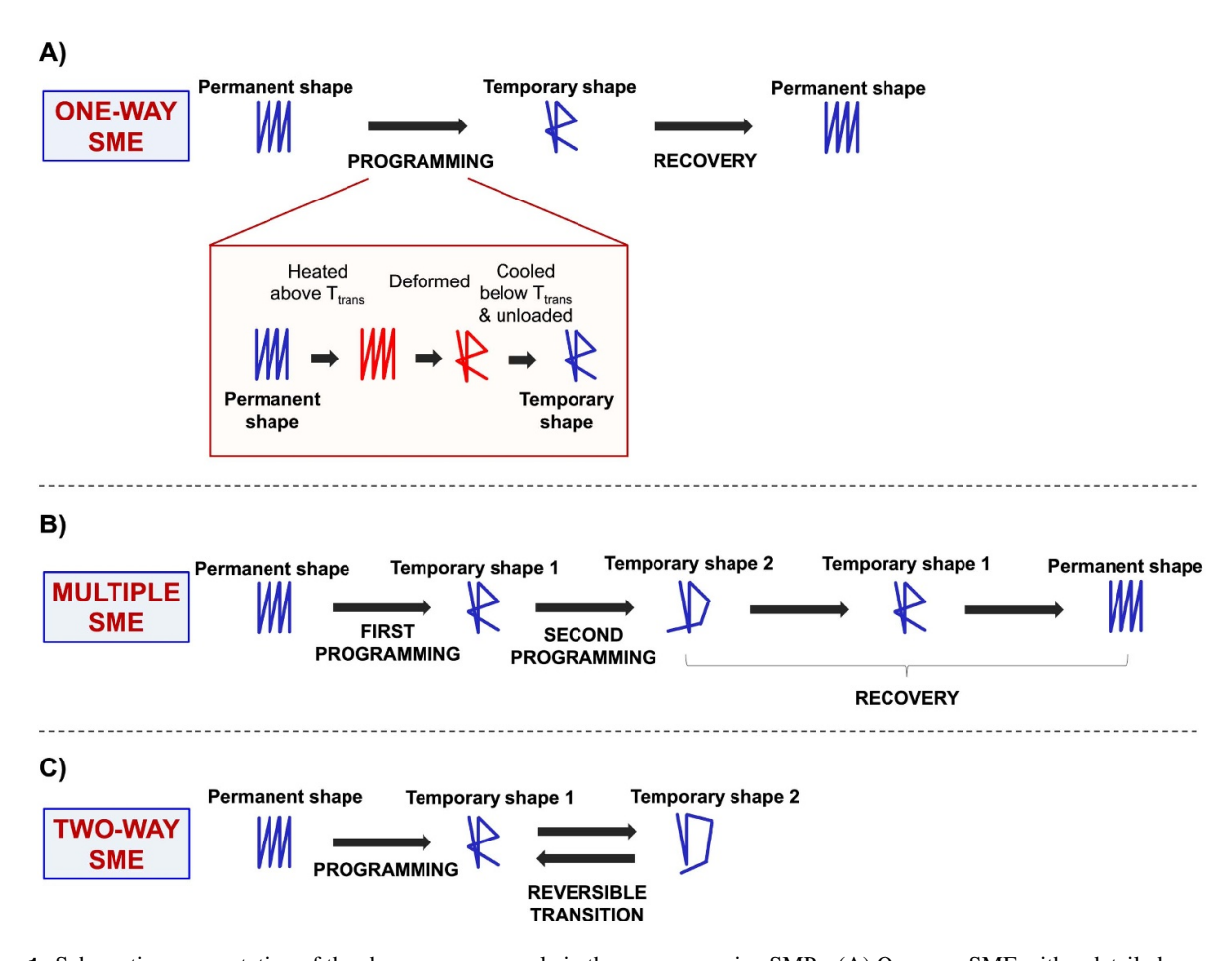


**Figure 1.** Schematic representation of the shape-memory cycle in thermo-responsive SMPs. (A) One-way SME with a detailed zoom of the programming step; (B) multiple SME; (C) two-way SME. Adapted from [2]. CC BY 4.0.

Table 1. Common Radial Basis Functions (RBF) with global and compact support.

Compactly supported RBF	Abbreviation	$\phi(\zeta)$
Wendland $C^0$	C0	$(1-\epsilon\zeta)^2$
Wendland $C^2$	C2	$(1 - \epsilon \zeta)^4 (4\epsilon \zeta + 1)$
Wendland $C^4$	C4	$(1 - \epsilon \zeta)^6 \left(\frac{35}{3} \epsilon \zeta^2 + 6\epsilon \zeta + 1\right)$
Globally supported RBF	Abbreviation	$\phi(\zeta)$
Polyharmonic spline	PHS	$r^n$ , $n$ odd
		$r^n \log(r)$ , n even
Thin plate spline	TPS	$r^2 \log(r)$
Multiquadric biharmonics	MQB	$\sqrt{a^2+(\epsilon r)^2}$
Inverse multiquadric biharmonics	IMQB	$\frac{\sqrt{a^2 + (\epsilon r)^2}}{\sqrt{a^2 + (\epsilon r)^2}}$ $1 + (\epsilon r)^2$
Quadric biharmonics	QB	$1+(\epsilon r)^2$
Inverse quadric biharmonics	IQB	$\frac{1}{1+(\epsilon r)^2}$ $e^{-\epsilon r^2}$
Gaussian biharmonics	GS	$e^{-\epsilon r^2}$

points—must be solved [8]. Once these coefficients are obtained, the displacement of any mesh node, whether within (interpolation) or outside (extrapolation) the domain, can be computed as the weighted sum of the radial contributions from all source points. This approach enables the definition of spatial displacements at known points and their projection onto

the entire mesh, resulting in a deformation that preserves the original grid topology [9].

The interpolation function comprises both a radial basis term  $\phi$  and a polynomial term h, the degree of which depends on the type of basis function used. The polynomial component guarantees exact reproduction of rigid body motions, thereby

enhancing the approximation's accuracy. If *N* is the number of source points, the RBF interpolant is expressed as:

$$s(\mathbf{x}) = \sum_{i=1}^{N} \gamma_i \phi(\|\mathbf{x} - \mathbf{x}_{k_i}\|) + h(\mathbf{x}). \tag{1}$$

Interpolation is feasible if the coefficients and polynomial weights can be determined such that the interpolant exactly reproduces the known values at the source points. Moreover, including the polynomial in the interpolant introduces an orthogonality condition, which ensures the system remains square:

$$s(\mathbf{x}_{k_i}) = g_i, \quad 1 \leqslant i \leqslant N \quad \text{and} \quad \sum_{i=1}^{N} \gamma_i p(\mathbf{x}_{k_i}) = 0 \quad (2)$$

for all polynomials p of degree less than or equal to that of h. A unique interpolant exists if the chosen basis is conditionally positive definite [10]. When a spline kernel is chosen, if its degree satisfies  $m \le 2$  [9], a linear polynomial of the form

$$h(\mathbf{x}) = \beta_1 + \beta_2 x_1 + \beta_3 x_2 + \dots + \beta_{n+1} x_n, \qquad \mathbf{x} \in \mathbb{R}^n \quad (3)$$

suffices. The resulting system of equations can be compactly represented in matrix form, which facilitates numerical implementation:

$$\begin{bmatrix} \mathbf{M} & \mathbf{P} \\ \mathbf{P}^{\mathrm{T}} & \mathbf{0} \end{bmatrix} \begin{Bmatrix} \gamma \\ \beta \end{Bmatrix} = \begin{Bmatrix} \mathbf{g} \\ \mathbf{0} \end{Bmatrix}. \tag{4}$$

Here,  $\mathbf{g}$  is the vector of known function values at the source points. The interpolation matrix  $\mathbf{M}$  is defined by:

$$M_{ij} = \phi\left(\left\|\mathbf{x}_{k_i} - \mathbf{x}_{k_i}\right\|\right), \quad 1 \leqslant i, j \leqslant N. \tag{5}$$

The constraint matrix **P** contains the spatial coordinates of the source points:

$$\mathbf{P} = \begin{pmatrix} 1 & x_{k_1} & y_{k_1} & z_{k_1} \\ 1 & x_{k_2} & y_{k_2} & z_{k_2} \\ \vdots & \vdots & \vdots & \vdots \\ 1 & x_{k_N} & y_{k_N} & z_{k_N} \end{pmatrix}.$$
(6)

Once the coefficients and weights are determined, the displacement components in the x, y, and z directions at a given point  $\mathbf{x}$  can be evaluated as follows [11]:

$$\begin{cases} S_{x}(\mathbf{x}) = \sum_{i=1}^{N} \gamma_{i}^{x} \phi(\|\mathbf{x} - \mathbf{x}_{k_{i}}\|) + \beta_{1}^{x} + \beta_{2}^{x} x_{1} + \beta_{3}^{x} x_{2} + \beta_{4}^{x} x_{n} \\ S_{y}(\mathbf{x}) = \sum_{i=1}^{N} \gamma_{i}^{y} \phi(\|\mathbf{x} - \mathbf{x}_{k_{i}}\|) + \beta_{1}^{y} + \beta_{2}^{y} x_{1} + \beta_{3}^{y} x_{2} + \beta_{4}^{y} x_{n} \\ S_{z}(\mathbf{x}) = \sum_{i=1}^{N} \gamma_{i}^{z} \phi(\|\mathbf{x} - \mathbf{x}_{k_{i}}\|) + \beta_{1}^{z} + \beta_{2}^{z} x_{1} + \beta_{3}^{z} x_{2} + \beta_{4}^{z} x_{n} \end{cases}$$

RBF have a wide range of applications, extending well beyond their original purpose of interpolating complex fields [12]. They are utilized in neural networks, where Gaussian kernels are commonly employed [13], in surface reconstruction from scattered data such as point clouds [14], and in the approximation of PDE solutions. Notably, RBF form the foundation

of the Kansa method [15, 16], a collocation technique that leverages the recursive differentiability of certain RBF kernels to compute numerical solutions to PDE systems. This approach enables the solution of challenging problems across various domains, from the continuum mechanics of composite materials [17] to heat conduction in nonhomogeneous media [18].

#### 3. Materials and methods

This section presents, first, the computational workflow proposed in this work, then the investigated case study and the numerical approaches employed to perform the simulations.

#### 3.1. Computational workflow

As previously discussed, one of the main challenges in numerically simulating the shape-memory cycle of an SMP lies in the programming step, during which the structure in its undeformed, permanent configuration must be deformed to assume the temporary shape. In most cases, the temporary shape is pre-determined, either resulting from manual deformation or corresponding to a known geometry that is required for functional purposes, such as activating a mechanism.

Generally, transforming the permanent configuration into the desired temporary shape is a complex and time-consuming task. It typically relies on a trial-and-error procedure, in which multiple boundary conditions must be iteratively adjusted to achieve a satisfactory match with the target geometry. In some cases—particularly for thin or highly deformable structures—this process cannot be completed in a single step. Instead, boundary conditions must be applied sequentially in multiple stages to prevent convergence issues arising from large deformations, snap-through phenomena, or structural instabilities [19]. The manual process of determining the deformed shape depends on several intangible factors, including the user's experience and skill, the clarity of the model, and, not least, a degree of luck. A key advantage of the proposed method is its ability to eliminate this element of uncertainty, replacing the trial-and-error nature of the preliminary stage with a deterministic and systematic approach.

In figure 2 a typical workflow, in which this approach is employed for the programming stage through mechanical deformation, is shown. The iterative process required to identify suitable boundary conditions (loads and displacements) to bring the permanent geometry to the temporary shape can be very time consuming and requires user input. In figure 3 the workflow proposed in this work is shown.

A geometrical computer-aided design representation of the temporary shape is generally available in application-driven problems, and can be easily reconstructed otherwise. The two geometries, permanent and temporary, are superimposed in space and a projection field is generated from one to the other with the aim of establishing a point-wise correspondence. A displacement field is first computed by projecting each edge curve from the permanent geometry onto the corresponding curve of the temporary configuration. This mapping is then

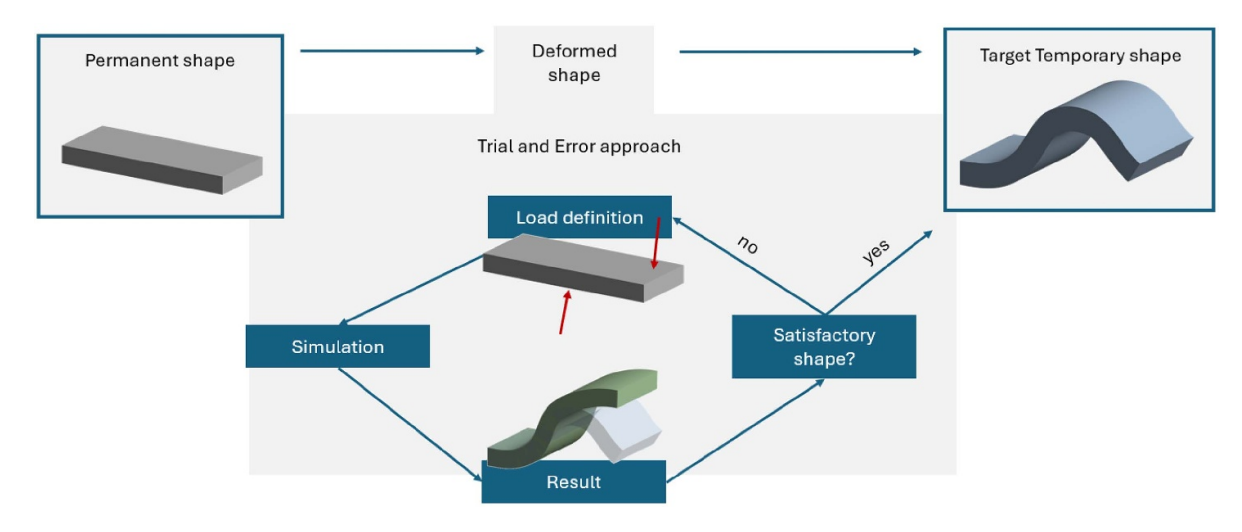
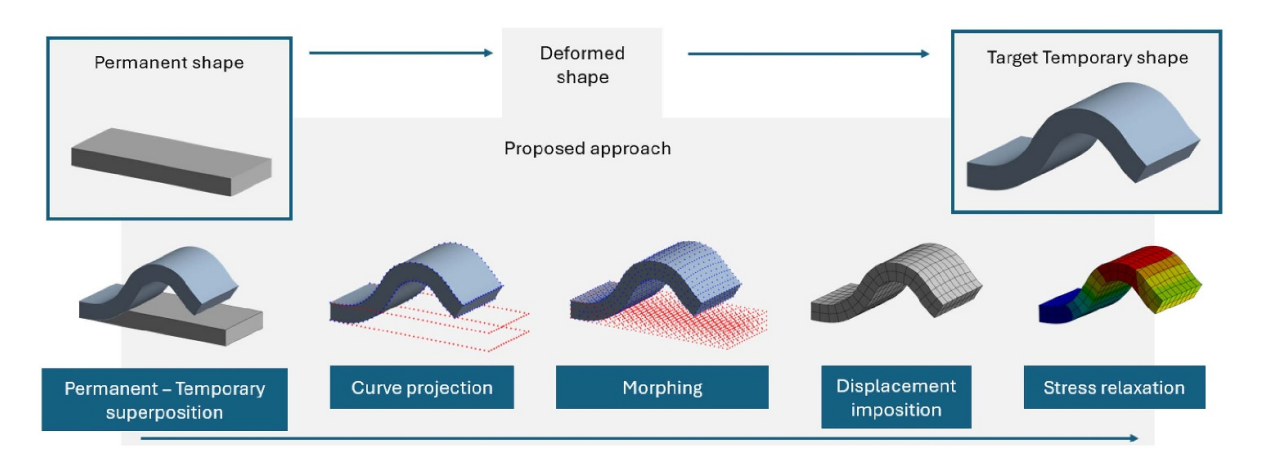
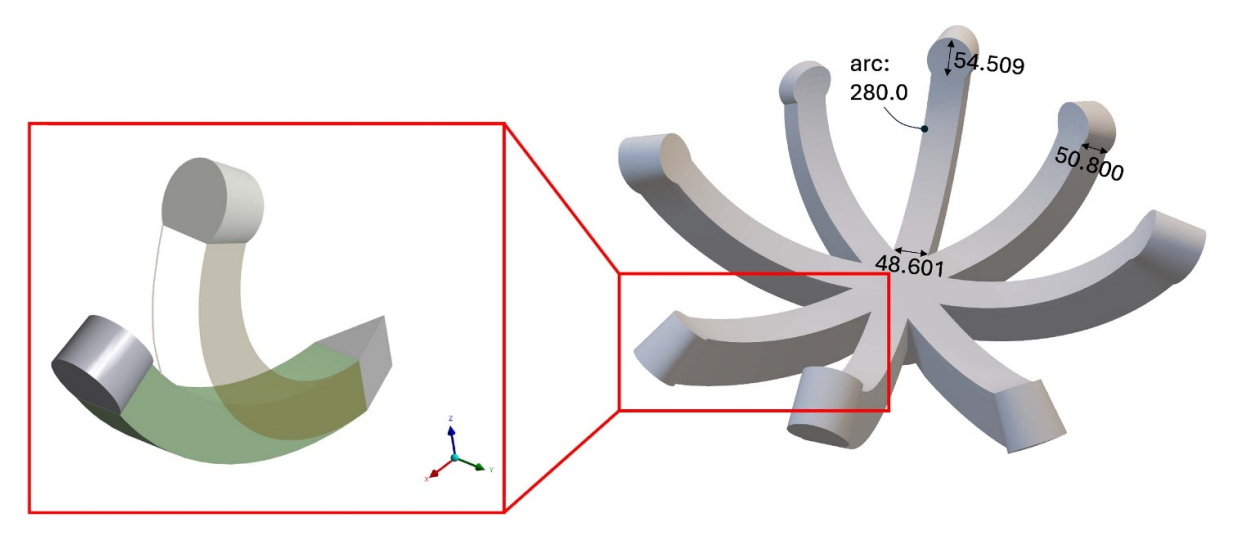


Figure 2. Trial-and-error approach to shape targeting.



**Figure 3.** Proposed approach to shape targeting using morphing.

extended to the surfaces by propagating the displacement field from the boundaries inward. As a result, the surfaces of the permanent shape are deformed to closely approximate those of the temporary shape. To refine the result and bring the deformed geometry even closer to the target, a second projection step is applied, this time along the normals of the target surface, ensuring improved alignment. The final displacement field is then extended to the full volume, yielding a volumetric morphing field. This geometrically derived morphing field is applied as a prescribed displacement boundary condition in a finite element simulation, where each node in the domain is displaced accordingly. It is important to note that the output of the RBF Morph tool consists of nodal displacements, which are then applied in a large-deformation finite element analysis. As a result, the deformed configuration of the mesh is technically achieved through the finite element simulation driven by physical laws—rather than by the RBF interpolation itself. Nevertheless, RBF Morph was chosen for this initial stage due to its ability to provide precise control over displacements and to leverage auxiliary geometries in generating the displacement field. However, since the deformation field is based solely on geometric considerations—without accounting for the material's physical response—it often results in non-physical strain distributions and significant stress concentrations, particularly in regions of high curvature or sharp transitions. To mitigate these artifacts and restore a physically realistic configuration, a subsequent stress relaxation step is introduced, allowing the structure to redistribute internal forces in accordance with the material behavior. This process is carried out in two steps using transient finite element simulations involving large deformations. When simulating the physical deformation of a model from the permanent to the temporary configuration—mimicking, for instance, manipulation via tools such as tweezers or actuators—certain regions of the geometry must remain fixed in space, while others are allowed to relax. In the first step, the entire geometry is initially held fixed, except for the regions that correspond to the areas in contact with the tools in the final configuration. These zones are released, enabling the structure to redistribute internal stresses and partially relax the material while preserving the intended spatial constraints. In the second step, the previously released tool-contact surfaces are fixed in space, and the rest of the geometry is freed. This allows the structure to settle into its final shape, eliminating artificial stress peaks



**Figure 4.** Right: full geometry from [13]. Left: zoom of the permanent (bloomed) geometrical shape of a single petal (green) with the temporary (de-bloomed) shape overimposed. All dimensions are in  $\cdot 10^{-3}$  mm.

and non physical strain concentrations throughout the domain. This two-stage approach ensures a smooth transition to the desired temporary shape while maintaining physical consistency in the mechanical response of the material.

After this mechanical step, the remaining steps of shapeprogramming are performed to fix the temporary shape. Accordingly, the obtained deformed shape is subjected to uniform cooling under fixed deformation. At the end of cooling, the mechanical load is then removed.

Finally, to complete the shape-memory cycle the fixed temporary shape is heated again to ensure the recovery of the initial permanent shape.

All the presented workflow will be applied and detailed for a representative case study in the next section. To conclude this section, we emphasize several requirements of the proposed procedure, which may pose limitations in certain cases. First, a deformed geometry representing the temporary shape is required to generate the initial displacement field. The accuracy and physical consistency of this geometry directly influence the ease and stability of the subsequent transient analysis. However, it is worth noting that such a geometry is typically available from the design phase, as SMP installations are usually application-driven and their shapes are predefined. In the case presented later in the paper, we constructed the temporary shape while maintaining a constant length of the petal's bending neutral plane. This approach ensured physical consistency and helped reduce both the complexity and duration of the transient analysis by minimizing stored elastic energy. Another key requirement is that the baseline and deformed geometries must share the same topology—that is, the same number of surfaces and edges—to enable a one-to-one correspondence and facilitate straightforward node mapping. This condition is generally met in SMP applications, as the transformation between permanent and temporary configurations typically involves simple bending or torsion, without drastic alterations to the overall geometry.

# 3.2. Case study

The case study analyzed here, and shown in figure 4(right), is taken from [13]. The structure consists of a 4D printed flower used for gripping purposes, whose original (permanent) shape is in a blooming configuration. The structure is made of an SMP exhibiting the one-way SME, as synthesized in [13] (denoted as 'ink formulation 2'). The transition temperature corresponds to the material's glass transition temperature, T<sub>g</sub>, which is 42 °C. The shape-memory performance is evaluated through a programming step followed by recovery. Specifically, programming involves deforming the permanent blooming shape at a temperature of  $80^{\circ}C > T_g$  to obtain a temporary de-bloomed shape. The de-bloomed shape allows the structure to grip an object. Figure 4(left) shows the permanent and temporary shapes of a single petal of the flower. The deformed configuration is then fixed by cooling down to  $25\,^{\circ}\text{C} < T_{\text{g}}$ , and, after removing the applied load, shape recovery is triggered by reheating the structure to  $80^{\circ}\text{C} > T_{\text{g}}$ . The recovery ensures the release of the gripped object.

# 3.3. Geometrical modeling and mesh

For our purposes, only one petal of the flower is studied exploiting symmetry (figure 4). The geometry is meshed by using 1120 eight-node linear isoparametric tetrahedral elements with full integration (Abaqus designation C3D8) and 30 six-node linear isoparametric triangular prism elements with full integration (Abaqus designation C3D6) (figure 5). A mesh convergence study was performed to validate mesh discretization.

#### 3.4. Constitutive model

The shape-memory behavior of the SMP under investigation is captured by using the three-dimensional finite-strain

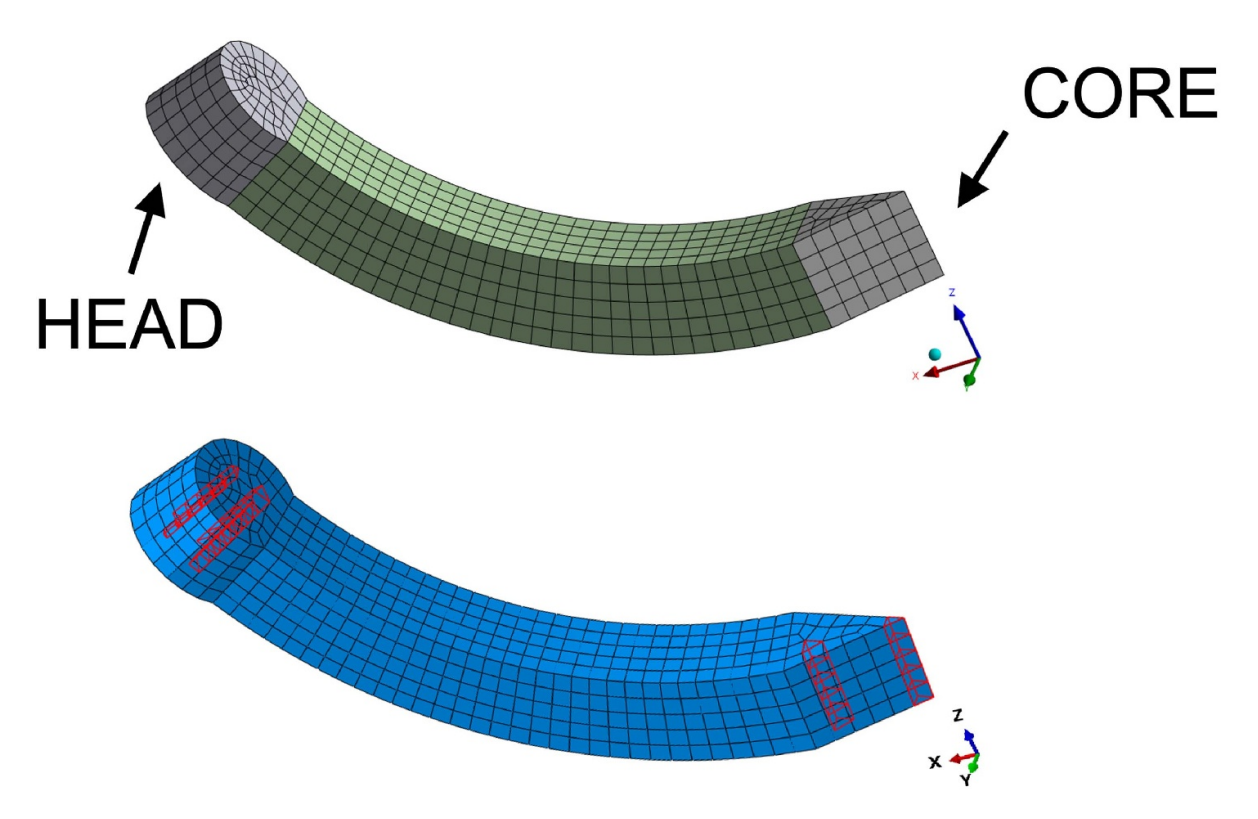


**Figure 5.** Top: numerical grid for the case study where the head and core of the petal are indicated in gray color. Bottom: numerical grid where six-node linear isoparametric triangular prism elements are highlighted in red color.

macroscopic constitutive model proposed by Boatti *et al* [20]. The model is based on a phase-transition approach and is able to describe the behavior of one-way SMPs based on the glass transition, including different material features as imperfect shape-fixing and incomplete shape-recovery. A brief overview of the main model features is presented below. The reader is referred to [20] for details on the model equations.

Briefly, the total deformation gradient F and temperature T are assumed as state variables. Then, proper phase variables are introduced to distinguish between the two material states (i.e. glassy and rubbery) within the SMP and related inelastic contributions: the scalar variable,  $z^g$ , describing the rubbery volume fraction, and the tensorial variables,  $\mathbf{F}^f$ ,  $\mathbf{F}^{pg}$  $\mathbf{F}^p$ , representing, respectively, the frozen deformation gradient, the plastic deformation gradient of the glassy phase, and the permanent deformation gradient. The Helmholtz specific free energy is determined by employing the rule of mixtures, considering that the material is a combination of rubbery and glassy phases. In particular, the hyperelastic responses of the rubbery and glassy phases are modeled through a Saint Venant-Kirchhoff type expression. Constitutive equations can be derived by applying a standard Coleman-Noll procedure on the Helmoltz free energy in a thermodynamic consistent framework. Evolution equations for the phase variables and related Kuhn Tucker conditions complete the model.

Model algorithm is implemented within a userdefined material subroutine for the finite element software ABAQUS/Standard (Simulia, Providence, RI).

Model parameters are calibrated on experimental data taken from [13] and are listed in table 2. Particularly, the Young's

modulus for the glassy and rubbery phases, respectively,  $E^g$ and  $E^{r}$ , are equal to the experimental storage modulus at low and high temperature, respectively; the Poisson's ratios for the glassy and rubbery phases, respectively,  $\nu^g$  and  $\nu^r$ , are taken from [20]; the transformation temperature,  $\theta_t$ , is equal to  $T_g$ ; the parameter defining half-width of the temperature range,  $\Delta\theta$ , and the transformation coefficient, w, are chosen considering that the recovery is generally completed at 55 °C for this SMP; the plastic hardening coefficient, h, and the stress limit,  $R_{\rm g}^{\rm p}$ , for plastic yielding of the glassy phase are taken from [21]. Given the very good shape-memory performances of the polymer under investigation, imperfect material behavior is not considered in the present work (i.e. coefficient c to tune imperfect shape-fixing is equal to one, while coefficient  $c_p$  to tune incomplete shape-recovery is equal to zero). This choice does not restrain the application of the proposed approach to other less-performant SMPs.

#### 3.5. Analysis set-up

This section describes the set-up of the entire analysis, from the evaluation of the displacement field via mesh morphing up to the finite element simulation of the shape-memory cycle.

3.5.1. Shape targeting set-up. To generate the displacement field to be applied to the numerical grid during the programming phase—following the same approach described in section 3.1 — a two-step procedure is adopted using Ansys software. First, a geometry projection and mesh morphing step

Parameter	Symbol	Value	Units
Young's modulus of the glassy phase	$E_{\mathfrak{g}}$	1400	MPa
Young's modulus of the rubbery phase	$E_{\rm r}^{\circ}$	2.9	MPa
Poisson's ratio of the glassy phase	$ u_{\mathtt{g}}$	0.29	
Poisson's ratio of the rubbery phase	$ u_{ m r}$	0.49	
Transformation temperature	$ heta_{t}$	42	$^{\circ}\mathrm{C}$
Half-width of the temperature range	$\Delta  heta$	15	$^{\circ}\mathrm{C}$
Transformation coefficient	w	0.35	1/°C
Plastic hardening coefficient	h	0	МРа
Stress limit for plastic yielding of the glassy phase	$R_{g}^{p}$	10	MPa
Imperfect shape-fixing coefficient	c	1	_
Incomplete shape-recovery coefficient	$c_{p}$	0	_

**Table 2.** Constitutive model parameters adopted in the present work.

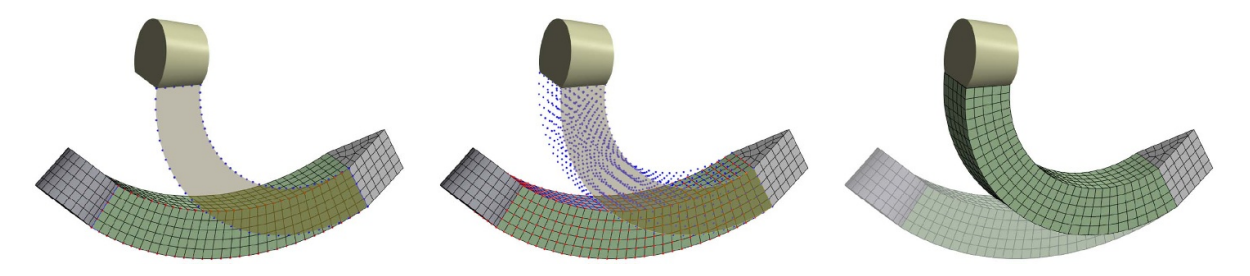


Figure 6. RBF set-up. Left: curve targeting. Center: volume propagation. Right: morphed mesh.

is performed, followed by a finite element simulation for stress relaxation. Taking advantage of the simple extruded geometry of the flower-like structure, as illustrated in figure 4, only the 2D profile of the temporary shape is used as the target geometry for morphing.

Each curve defining the body of the petal (see figure 6(left)) is projected onto its corresponding deformed 2D profile. This displacement is then propagated into the volume (center image), generating a set of RBF control points to guide the deformation of the entire mesh. During the morphing phase, the core of the petal is held fixed, while a rigid displacement is applied to the head, mimicking the physical manipulation expected in the real application. The resulting morphed configuration is shown in the rightmost image of figure 6.

The displacement field obtained through the morphing procedure is used as an initial prescribed boundary condition in a multistep transient finite element simulation aimed at stress relaxation. In the second step-following the strategy outlined in section 3.1 — the core and the main body of the petal are held fixed, allowing only the head region to relax. This step mitigates the artificial stress concentrations potentially introduced by the rigid translation imposed during morphing. In the third and final step, the head and core are fixed, replicating the real mechanical constraints during manipulation, while the remaining parts of the petal are released and allowed to relax. This ensured a physically-consistent stress distribution across the entire structure. To accelerate convergence of the transient simulation, critical damping is estimated for the system and applied to the material model of the petal. The final stressrelieved configuration of the petal is then used to compute the displacement field that serves as input for the SMP simulation cycle described in the following section.

3.5.2. Finite element analysis set-up. A quasi-static mechanical analysis is performed by using the commercial finiteelement software ABAQUS/Standard to simulate the entire shape-memory cycle of the 4D printed structure under investigation (see section 3.2). The material model is described in section 3.4. The core of the flower (gray part in figure 5(right)) is kept fixed throughout all the analysis. Temperature conditions are applied uniformly over all the domain using the Abaqus command 'Predefined field'. The permanent blooming shape is first deformed to the temporary de-bloomed shape at 80°C. In order to obtain this target temporary shape, proper displacement boundary conditions are applied to each node of the mesh. The values of these displacements are derived from section 3.5.1. Then, in order to simulate the programming step, the deformed petal is cooled down to 25°C keeping the deformation fixed for the head of the petal (gray part in figure 5(left)). At 25°C, the petal is unloaded to fix the temporary shape. Finally, the temporary shape is re-heated up to 80°C under load-free conditions to induce recovery of the permanent blooming shape.

#### 4. Results

This section presents the results of the numerical simulations with special attention to the shape projection of the permanent shape onto the temporary one, as described in section 3.5.1.

Figure 7 illustrates the motion of the petal during the first step of the transient simulation, in which the displacement field obtained from the morphing procedure is applied as a prescribed boundary condition.

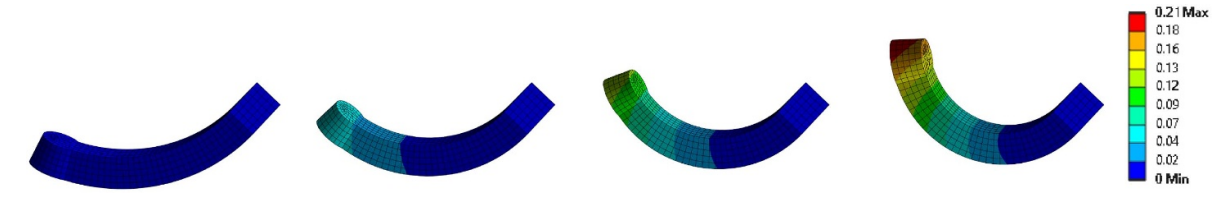


Figure 7. Petal motion [mm] during the transient simulation.

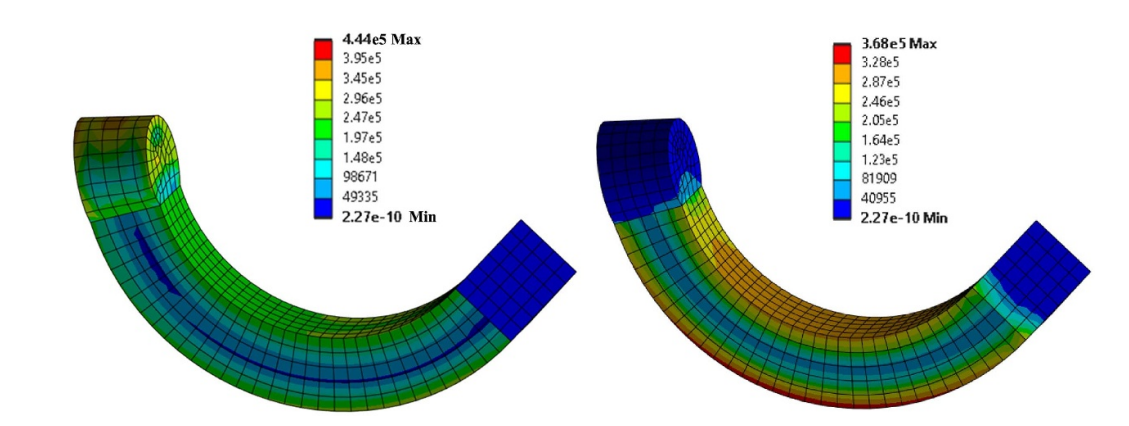


Figure 8. Contour plot of the von Mises stresses [MPa]. Left: stresses after morphing, Right: stresses after the relaxation procedure.

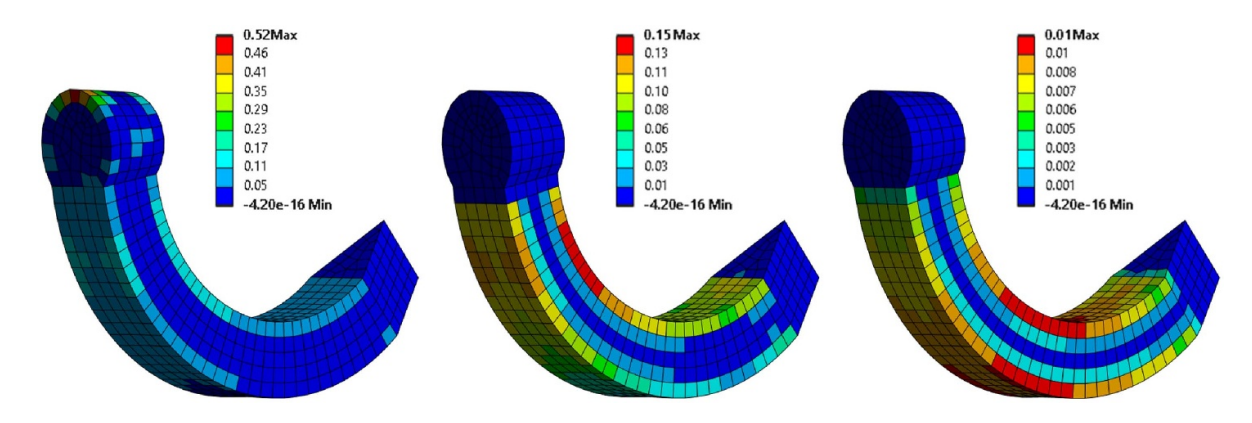


Figure 9. Strain energy [J] for the three steps.

As previously discussed, this motion introduces artificial and non-physical stresses, as the applied displacements are guided purely by geometric considerations through the morphing procedure. Nonetheless, the resulting configuration is already very close to the desired physical shape, which makes the subsequent stress relaxation procedure effective in removing these artifacts.

In figure 8(left), the von Mises stress distribution resulting from the morphing step is shown. Significant stress concentrations can be observed, particularly at the petal head where sharp spikes appear, features that are not physically justified. In contrast, the right-hand image in figure 8 shows the stress field after the relaxation procedure, with stresses nearly eliminated at both the head and the core. A butterfly-shaped distribution remains, primarily due to bending effects along the petal body.

During the two-step stress relaxation process, the artificial elastic energy introduced by morphing is gradually dissipated. The total strain energy immediately after the initial imposed displacement amounts to 49.8 J, as shown in figure 9(left). After the first relaxation step—where the petal head is released while the body and core are held fixed—this energy is reduced by approximately 30%, reaching 34.8 J (center), with the reduction localized mostly at the head.

In the final step, where the head and core are fixed and the rest of the petal is released, the strain energy drops further to just 3.8 J. This results in a smooth and physically consistent energy distribution, as depicted in figure 9(right).

Further, in order to provide an order of magnitude of the computational cost of the mesh morphing approach for the analyzed case, figure 10 shows the needed time versus number

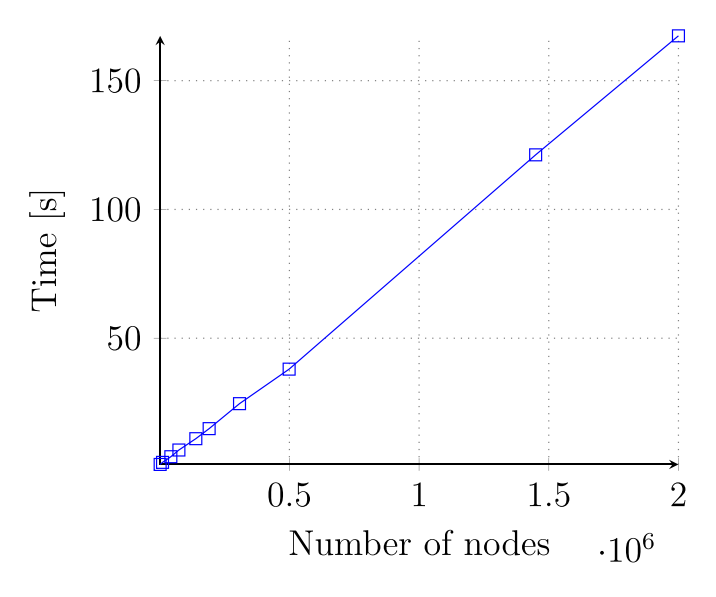
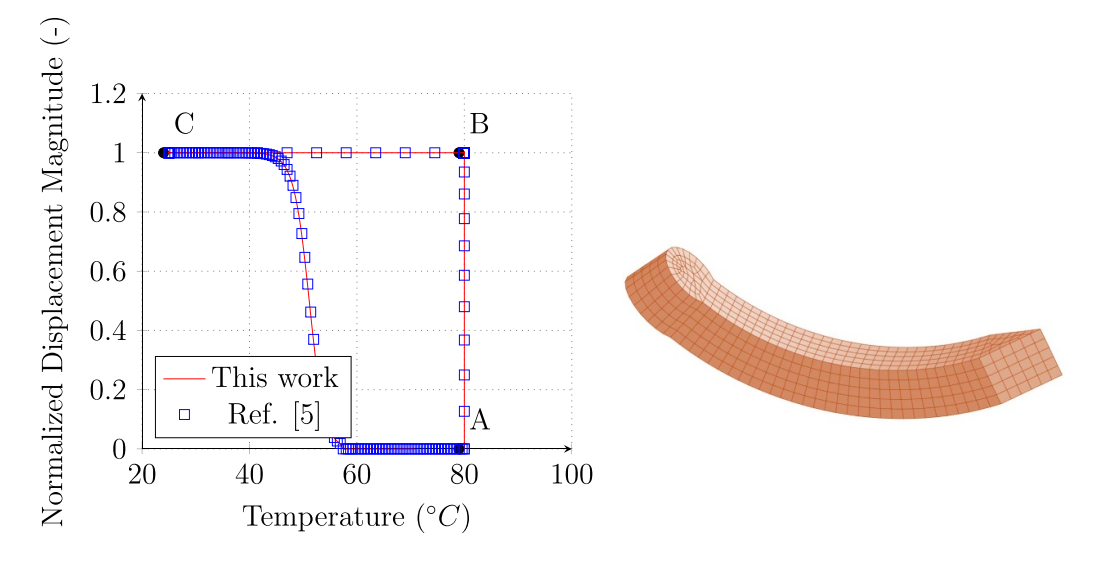


Figure 10. Time needed for mesh morphing versus number of nodes of the mesh.



**Figure 11.** Left: finite element results in terms of normalized displacement magnitude vs temperature for a node belonging to the head of the petal. Right: recovered shape after heating.

of mesh nodes diagram. As it can be seen, a linear trend can be observed.

Then, the finite element simulation described in section 3.5.2 allows to reproduce correctly the shape-memory cycle observed experimentally in [13]. Figure 11(left) reports the displacement magnitude (normalized with respect to its maximum value) versus temperature curve for a node belonging to the head of the petal. The programming step starts at 80°C (point A) and ends at 25°C (point C). Heating from point C to point A induces recovery. As it can be seen, the de-blooming flower shape starts opening between 43°C and 48°C. The full recovery takes place at 55°C (figure 11(right)). For increasing temperatures the recovery is complete and no further phenomena are observed. The curve obtained in the present work is also compared to the one obtained numerically

in [13] for the same test case, demonstrating the accuracy of the results.

The obtained results demonstrate the effectiveness of the proposed approach in supporting the design and simulation of SMP-based structures.

# 5. Conclusions

This paper has presented a novel computational approach based on finite elements and mesh morphing to support the simulation of the shape-memory cycle typical of SMP-based structures.

The work has been motivated by the current difficulties encountered in accurately reproducing the target temporary shape. In fact, identifying the correct boundary conditions to deform an initial geometry into a desired target shape involves a trial-and-error process, often requiring multiple tentative simulations and significant manual effort. This can result in time-consuming workflows, often leading to a final shape not exactly comparable to the target one.

The approach has been applied here to the simulation of a 4D-printed structure. Results have demonstrated that mesh morphing allows the user to directly impose the desired temporary shape, thus bypassing the need to determine complex boundary condition setups, lowering human intervention and setup time. Additionally, the requirements of the proposed procedure have been discussed, including the need for a deformed geometry-typically available from the design phase-and for the same topology of the baseline and and of deformed geometries.

Moreover, it is worth highlighting that the work has focused on one-way SMPs, but the approach can be applied to other types of SMPs, being the temporary shape a feature of all SMEs. Accordingly, the constitutive model used in the present work is used only for simulation purposes, but can be replaced by any other macroscopic model available from the literature.

Finally, this approach provides a valuable tool for the design and optimization of SMP systems and, as future extensions, it shows promise for application to cases involving contact interactions or large deformations.

# Data availability statement

The data that support the findings of this study are openly available at the following URL/DOI: it will be made available at https://doi.org/10.5281/zenodo.15754028.

# **Acknowledgments**

This work was funded by the European Union ERC CoDe4Bio Grant ID 101039467. Views and opinions expressed are however those of the author(s) only and do not necessarily reflect those of the European Union or the European Research Council. Neither the European Union nor the granting authority can be held responsible for them.





European Research Council

#### **ORCID iD**

Giulia Scalet © 0000-0001-7683-566X

#### References

- [1] Xia Y, He Y, Zhang F, Liu Y and Leng J 2021 A review of shape memory polymers and composites: mechanisms materials and applications *Adv. Mater.* **33** 2000713
- [2] Scalet G 2020 Two-way and multiple-way shape memory polymers for soft robotics: an overview *Actuators*
- [3] Bonetti L and Scalet G 2025 4D fabrication of shape-changing systems for tissue engineering: state of the art and perspectives *Prog. Addit. Manuf.* 10 1913–43
- [4] Yan C and Li G 2022 Tutorial: thermomechanical constitutive modeling of shape memory polymers *J. Appl. Phys.* 131 111101
- [5] Porziani S, Groth C, Waldman W and Biancolini M E 2021 Automatic shape optimisation of structural parts driven by BGM and RBF mesh morphing *Int. J. Mech. Sci.* 189 105976
- [6] Chiappa A, Groth C and Biancolini M E 2023 A two-scale RBF meshless method for the interface stress retrieval in simply bended and torqued long-fibres laminates *Compos.* Struct. 306 116600
- [7] De Boer A, Van der Schoot M S and Bijl H 2007 Mesh deformation based on radial basis function interpolation Comput. struct. 85 784–95
- [8] Buhmann M D 2000 Radial basis functions Acta Numer. 9 1–38
- [9] Beckert A and Wendland H 2001 Multivariate interpolation for fluid-structure-interaction problems using radial basis functions *Aerosp. Sci. Technol.* 5 125–34
- [10] Micchelli C A 1984 Interpolation of Scattered Data: Distance Matrices and Conditionally Positive Definite Functions (Springer) pp 143–5
- [11] Biancolini M E 2017 Fast Radial Basis Functions for Engineering Applications (Springer)
- [12] Biancolini M E, Chiappa A, Giorgetti F, Groth C, Cella U and Salvini P 2018 A balanced load mapping method based on Radial Basis Functions and Fuzzy Sets *Int. J. Numer. Methods Eng.* 115 1411–29
- [13] Wang Y, Sachyani Keneth E, Kamyshny A, Scalet G, Auricchio F and Magdassi S 2022 4D multimaterial printing of programmable and selective light-activated shape-memory structures with embedded gold nanoparticles Adv. Mater. Technol. 7 2101058
- [14] Drake K P, Fuselier E J and Wright G B 2022 Implicit surface reconstruction with a curl-free radial basis function partition of unity method SIAM J. Sci. Comput. 44 A3018–40
- [15] Kansa E J 1990 Multiquadrics—A scattered data approximation scheme with applications to computational fluid-dynamics—I surface approximations and partial derivative estimates *Comput. Math. Appl.* 19 127–45
- [16] Kansa E J 1990 Multiquadrics—A scattered data approximation scheme with applications to computational fluid-dynamics—II solutions to parabolic, hyperbolic and elliptic partial differential equations *Comput. Math. Appl.* 19 147–61
- [17] Chiappa A, Groth C, Reali A and Biancolini M E 2020 A stress recovery procedure for laminated composite plates based on strong-form equilibrium enforced via the RBF Kansa method *Compos. Struct.* 244 112292
- [18] Popczyk O and Dziatkiewicz G 2022 Kansa method for solving initial-value problem of hyperbolic heat conduction in nonhomogeneous medium *Int. J. Heat Mass Transfer* 183 122088

- [19] Groth C, Chiappa A, Porziani S, Salvini P and Biancolini M E 2022 An RBF meshless approach to evaluate strain due to large displacements in flexible printed circuit boards *Micromachines* 13 1163
- [20] Boatti E, Scalet G and Auricchio F 2016 A three-dimensional finite-strain phenomenological model for shape-memory polymers: formulation, numerical simulations and
- comparison with experimental data *Int. J. Plast.* **83** 153–77
- [21] Sachyani Keneth E, Lieberman R, Rednor M, Scalet G, Auricchio F and Magdassi S 2020 Multi-material 3D printed shape memory polymer with tunable melting and glass transition temperature activated by heat or light *Polymers* 12 710